

# Conformational disorder and dynamics of proteins sensed by Raman optical activity

*Carl Mensch<sup>†,‡</sup>, Patrick Bultinck<sup>‡</sup> and Christian Johannessen<sup>†\*</sup>*

<sup>†</sup>. Department of Chemistry, University of Antwerp, Groenenborgerlaan 171, B-2020

Antwerp, Belgium.

<sup>‡</sup>. Department of Chemistry, Ghent University, Krijgslaan 281 (S3), B-9000 Ghent, Belgium.

**ABSTRACT** Raman optical activity (ROA) spectra of proteins hold a lot of information about their structure in solution. To elucidate the ROA spectra of the intrinsically disordered proteins (IDPs), involved in neurodegenerative diseases, the effect of conformational disorder and dynamics on the ROA spectra was studied. Density functional theory (DFT) computations of small ensembles of model peptides with increasing disorder show that the ROA patterns of  $\alpha$ -helical and poly-proline II (PPII) structure reflect the average backbone angles in the ensemble. While the amide III region in the ROA of the  $\alpha$ -helical peptides is shown to be surprisingly robust with disorder, the amide III region of PPII secondary structure diminishes in intensity with increasing structural disorder. The results show that the ROA spectra of IDPs hence more likely stem from short stretches of well-defined PPII helices rather than a very flexible chain. Further DFT computations support that mixing of PPII with helical secondary structure is consistent with experimental spectra of IDPs, while mixing with  $\beta$ -strand results in spectral

patterns that are not observed experimentally. The detailed information obtained from these results contributes to a better understanding of the spectrum-structure relation.

## INTRODUCTION

Over the past decades, Raman optical activity (ROA) has been shown to be a spectroscopic technique that is uniquely sensitive to the solution structure of biomolecules.<sup>1,2</sup> Nevertheless, its use as a complementary structural elucidation technique in structural biology is not widespread. Exactly because of this strong structural sensitivity, the detailed interpretation of the spectroscopic signals is very challenging. Since ROA provides unique spectral patterns for *inter alia* peptides,<sup>3</sup> proteins<sup>1</sup>, glycoproteins<sup>4,5</sup> and intrinsically disordered proteins (IDPs)<sup>6,7</sup> there is a clear incentive to create a deeper understanding of the structure-spectrum relationship. Especially proteins such as IDPs are challenging to characterize by standard techniques.<sup>8</sup> As these proteins are involved in neurodegenerative disorders such as Alzheimer's and Parkinson's disease, there is a strong motivation to develop structure elucidation techniques that are complementary to for example nuclear magnetic resonance (NMR) methodologies.<sup>8</sup>

The strength of Raman spectroscopies in the study of dynamic systems stems from the very short time scale of the scattering process ( $\sim 3.3 \times 10^{-14}$  s for a vibration with wavenumber  $1000 \text{ cm}^{-1}$ ) which is much smaller than that of conformational changes.<sup>9</sup> The spectra are therefore a superposition of snap-shot spectra arising from all conformations that the protein adopts in solution. Conventional Raman spectra of proteins arise from molecular vibrations in both the side-chains as well as the backbone of the protein. ROA on the other hand is measured as the difference in the right- ( $I_R$ ) and left-handed ( $I_L$ ) circularly polarized components in Raman scattered light and as such only picks up signals arising from rigid and chiral parts of the protein.

Therefore, the experimentally observed ROA spectral patterns mainly arise from amide bond and skeletal stretching vibrations in the backbone of the protein and thus depend on the secondary structure of the protein.<sup>1</sup> While the most important secondary structure elements such as  $\alpha$ -helix and  $\beta$ -sheet can readily be identified from a protein's ROA spectrum, the detailed interpretation of ROA spectra is elusive.<sup>10</sup>

Recently, our group reported the creation of a ROA database that provides the relation between the secondary structure and the corresponding ROA patterns.<sup>10</sup> The database consists of a large collection of calculated ROA spectra, each corresponding to a single secondary structure model. Using that database, the experimental ROA patterns of various peptides adopting a specific secondary structure in solution could be elucidated. Interestingly, the database also correctly assigns the secondary structure of the flexible XAO peptide that has an important conformational propensity to poly-L-proline type II helix (PPII), yet is considered to be flexible and explore multiple regions of the Ramachandran space.<sup>10,11</sup> A PPII helix is characterized by the backbone  $\phi$  and  $\psi$  torsion angles clustering around  $\phi = -75^\circ$  and  $\psi = 145^\circ$  in the Ramachandran plot and is also observed for sequences that do not contain proline.<sup>11</sup> It is an important secondary structure element of both globular proteins and flexible and dynamic IDPs.<sup>11</sup> Since our ROA database considers fixed model geometries with a regular arrangement of backbone torsion angles (the same  $\phi/\psi$  angles for each residue in the backbone), there is a need to further understand the effect of conformational dynamics and disorder on the ROA spectra of peptides and proteins. To this end, using Density Functional Theory (DFT), the ROA spectrum was firstly computed for a peptide model with a fixed backbone conformation by setting the  $\phi$  and  $\psi$  angles of all residues in its sequence the same values across the backbone. Next, the effect of conformational dynamics and disorder was investigated by increasingly deviating the conformation of this peptide from

the original regular conformation and monitoring the effect on the computed ROA spectrum. In this study, the effect of conformational dynamics on the ROA spectra of the left-handed PPII helix and the right-handed  $\alpha$ -helix was studied, since ROA has been shown to be very sensitive to these types of secondary structure, yet the detailed understanding of their spectral characteristics is still lacking.<sup>10</sup> Furthermore, these secondary structure types are of interest to elucidate the experimental ROA spectra of IDPs.<sup>7</sup>

## METHODOLOGY

ROA signals of proteins mainly arise from the amide and skeletal stretching vibrations in the backbone, therefore poly-L-alanine peptides are often used in computational ROA studies since this is the smallest chiral amino acid and conformational averaging of the side-chains does not need to be considered.<sup>10</sup> In this study, model peptide structures of the general formula  $\text{HCO}-(\text{L-Ala})_7\text{-NH}_2$  were created using the Python peptide builder by Tien *et al.* that generates the models based on a set of  $\phi$  and  $\psi$  torsion angles.<sup>12</sup> Firstly, different secondary structure element models were created by setting the torsion angles the same for each residue in each peptide model. To include conformational dynamics, the model  $\phi$  and  $\psi$  angles were varied to different extents from the initial angles. To this end, the torsion angles of each residue were generated using the “randn” function in Matlab R2017a (Mathworks, Inc.) that renders normally distributed pseudorandom numbers. By increasing the standard deviation of these random numbers, the generated  $\phi$  and  $\psi$  angles deviate more and more from the initial chosen angles, and hence more and more conformational variation is imposed on the model peptide. In this way, families of 50 randomly generated conformations were constructed where for each family, respectively a different degree of conformational freedom was imposed by setting the standard deviation  $\sigma$  of the torsion angles to 6, 10, 20 or 30.

Next, the geometry of each conformation of the model peptide was partially optimized using the normal mode optimization procedure.<sup>13</sup> By locking the normal modes below 300 cm<sup>-1</sup> in the optimization, the backbone conformation is retained, while the modes of spectroscopic interest are fully relaxed.<sup>13</sup> These geometry optimizations were performed using the B3PW91 DFT functional and the 6-31G(d,p) basis set. Subsequently, the Hessian and Raman and ROA tensors were calculated using the same functional and the 6-31++G(d,p) basis set. The backscattered Raman and ROA spectra were constructed by using a Lorentzian function for each normal mode with a full width at half height of 20 cm<sup>-1</sup> to mimic the physical line broadening in the experimental spectra. A Boltzmann distribution factor was used to correct for temperature (300 K).<sup>10</sup> Solvent-solute interactions with water were taken into account using the self-consistent reaction field model (scrf). For all DFT calculations, the Gaussian 16 (rev A.03) program was used.<sup>14</sup> For the sake of comparison with experimental data in scientific literature, the calculated spectra in this text are scaled in the wavenumber dimension by using a global scaling factor of 0.987.<sup>10</sup> Images of molecular structures were created using Jmol-12.2.32 or CylView v1.0 beta and figures were produced using Matlab R2017a.<sup>15,16</sup> The Ramachandran plots were prepared with “scatplot” in Matlab.

## **Results & Discussion**

### **Intrinsic disorder and the PPII secondary structure**

IDPs are very flexible proteins but many of their backbone torsion angles fluctuate around  $\phi = -75^\circ$  and  $\psi = 145^\circ$  characteristic for PPII secondary structure.<sup>11</sup> ROA gives unique spectral patterns of IDPs that support that these dynamic proteins do not behave like random coils but that they do contain residual structure.<sup>7,17,18</sup> The most prominent band ( $\sim 1320$  cm<sup>-1</sup>) in the

experimental ROA spectra of IDPs is assigned to arise from PPII secondary structure, while further understanding of the relation between the spectral patterns and a protein's structure is lacking.<sup>1,18,19</sup> Recently, our group reported the experimental ROA spectrum of the XAO peptide that is considered to primarily adopt PPII helical structure.<sup>10,11,20,21</sup> Yet, the XAO peptide is flexible and its radius of gyration was shown by small-angle X-ray scattering (SAXS) to be much smaller than that it would be for a fully extended PPII helix.<sup>21</sup> Zhu *et al.* suggested that this observation of a low radius of gyration could be reconciled with the strong evidence from spectroscopic methods pointing to a major contribution of PPII helical structure in the peptide, by proposing that stretches of PPII structures are truncated by other secondary structure elements.<sup>11,18</sup> We showed that the experimental ROA spectrum of the XAO peptide was very well reproduced by spectra calculated using DFT of poly-L-alanine model structures with a regular PPII backbone conformation; *i.e.* with all backbone torsion set to  $\phi = -75^\circ$  and  $\psi = 145^\circ$ .<sup>10</sup> This observation hence prompted us to further study how the spectral patterns would be affected by conformational dynamics or disorder, as both the XAO peptide and IDPs in general have a dynamic and flexible structure, although with a propensity for PPII conformation. In **Figure 1**, our approach to study this effect is illustrated. The Ramachandran plots in **Figure 1 (a)** show the distribution of the torsion angles going from  $\phi = -75^\circ \pm \sigma$  and  $\psi = 145^\circ \pm \sigma$  with a low standard deviation from the mean angles ( $\sigma = 6$ ) to much more conformationally randomized structures ( $\sigma = 30$ ). The Ramachandran plots show all the  $\phi$  and  $\psi$  backbone angles of the 50 conformations of each conformational family. The corresponding molecular geometries are displayed as superimposed stick figures in **Figure 1 (b)**. In the Raman and ROA spectra, the most variation is witnessed in the lower wavenumber region (200-800  $\text{cm}^{-1}$ ) and the extended amide III region (1240-1345  $\text{cm}^{-1}$ ) as shown in **Figure 1 (c)**. Although the individual spectra are

distinctly different, averaging of the spectra over the 50 conformations in each family leads to mean spectra with similar patterns. In **Figure 1 (d)**, the Raman and ROA spectra of HCO-(L-Ala)<sub>7</sub>-NH<sub>2</sub> with all backbone angles set to  $\phi = -75^\circ$  and  $\psi = 145^\circ$  (blue,  $\sigma = 0$ ) are compared to the mean spectra of the four conformational families ( $\sigma = 6, 10, 20, 30$  in red, yellow, purple and green, respectively). The conventional Raman spectral patterns are affected only to a very limited extent by the increasing conformational disorder. The most apparent changes are the broadening of the lower wavenumber region (200-800 cm<sup>-1</sup>), which leads to the lowering of the band maxima in that region.

ROA is more sensitive to the increase in conformational freedom. Both the low wavenumber region and the extended amide III region in the ROA spectra are strongly reduced in intensity with increasing conformational disorder of the HCO-(L-Ala)<sub>7</sub>-NH<sub>2</sub> peptide model. The ratio of the maximum intensity of the amide III relative to the amide I region is also reduced as the maximum intensity of the amide III region drops significantly with increasing disorder. This might be an indication that the relative ratio in experimental spectra of IDPs can be used as an indicator of the dynamics or conformational freedom of IDPs. For example, both the XAO peptide<sup>10</sup> (see above) and the IDP  $\alpha$ -synuclein<sup>7</sup> have a positive amide III band with a maximum intensity that is higher relative to the amide I maximum intensity in their experimental ROA spectra. The ROA spectra in **Figure 1** hence suggest that the standard deviation of the mean torsion angles of XAO and  $\alpha$ -synuclein in the PPII region of the Ramachandran plot is limited and lower than roughly  $\sigma = 20$ . This suggests that the ROA patterns of IDPs arise from short sequences in the protein adopting PPII conformation with torsion angles very close to  $\phi = -75^\circ$  and  $\psi = 145^\circ$ . Our results support the hypothesis that the XAO peptide adopts PPII helical

secondary structure truncated by other secondary structure elements and furthermore indicate that the variation of the backbone angles in the PPII region of the Ramachandran plot is limited.

To further investigate the effect of mixing different secondary structure elements, in following sections the effect of mixing PPII secondary structure with left-handed helical structure is evaluated. Before this mixing can be considered, in the next section, we first examine how the ROA patterns of  $\alpha$ -helical structure on its own are affected by increasing conformational disorder.



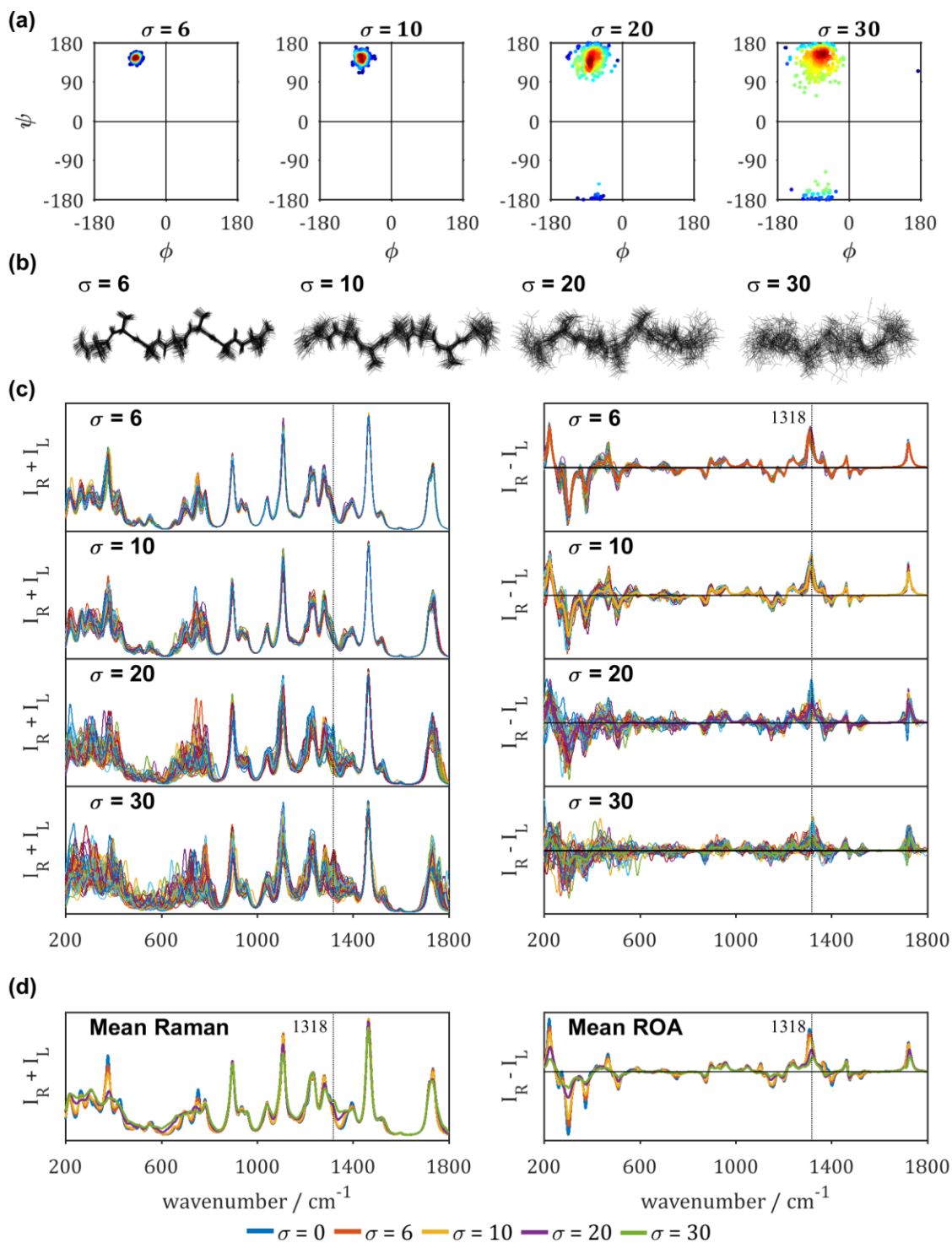


**Figure 1.** Effect of conformational disorder on the Raman and ROA patterns of PPII secondary structure. The backbone conformation of  $\text{HCO}-(\text{L-Ala})_7\text{-NH}_2$  is increasingly randomized by deviating each  $\phi$  and  $\psi$  angle in the backbone from  $\phi = -75^\circ$  and  $\psi = 145^\circ$  to  $\phi = -75^\circ \pm \sigma$  and  $\psi$

$= 145^\circ \pm \sigma$ . (a) Ramachandran plots displaying the increasing deviation from the mean angles  $\phi = -75^\circ$  and  $\psi = 145^\circ$  angles for each family of 50 structures with a set standard deviation  $\sigma$ . (b) Superposition of the 50 conformations of HCO-(L-Ala)<sub>7</sub>-NH<sub>2</sub> shown as stick figures for each family. The y-axes are set to the same limits. (c) Individual Raman ( $I_R+I_L$ ) and ROA ( $I_R-I_L$ ) spectra of each family of 50 conformations. (d) Mean Raman and ROA spectra of the four families ( $\sigma = 6$  (red), 10 (yellow), 20 (purple) or 30 (green) compared to the computed spectrum of HCO-(L-Ala)<sub>7</sub>-NH<sub>2</sub> with all backbone angles set to  $\phi = -75^\circ$  and  $\psi = 145^\circ$  (blue;  $\sigma = 0$ ).

### **The ROA patterns of left-handed helical structure.**

The ROA bands that mark  $\alpha$ -helical protein structure are well-studied and were assigned years ago.<sup>1,22</sup> The most distinctive patterns are a  $-/+$  couplet centered at  $\sim 1650\text{ cm}^{-1}$  in the amide I region and a  $-/+ +$  pattern at  $\sim 1245/1300/1345\text{ cm}^{-1}$  in the extended amide III region.<sup>1,10</sup> The relative ratios of the amide III bands of  $\alpha$ -helical proteins differ, which therefore has been suggested to be sensitive to the exact secondary structure. However, the detailed interpretation has been matter of debate in scientific literature. Already in 1999, Blanch *et al.* suggested that the positive band around  $1345\text{ cm}^{-1}$  ( $C\alpha$ -H bending vibration parallel to the C-N bond, coupled with amide III) marks hydrated helical structure, while the  $1300\text{ cm}^{-1}$  ( $C\alpha$ -H bending vibration perpendicular to the C-N bond, coupled with amide III) was proposed to be a signature of  $\alpha$ -helical structure without hydration.<sup>10,23,24</sup> These assignments were later questioned and shown to be inaccurate.<sup>10</sup> Nevertheless, our group showed that the ratio of the two bands is very sensitive to the exact helical geometry, which can be affected by intramolecular hydrogen bonding or interaction with the solvent.<sup>10</sup> The database developed in our group showed that helical structure with the C=O group tilting outwards from the helix axis, gives rise to a very intense ROA band around  $1300\text{ cm}^{-1}$ , while the band around  $1345\text{ cm}^{-1}$  is a conservative marker of  $\alpha$ -helical

structure. Since that database consists of regular conformations with repeated  $\phi$  and  $\psi$  angles, here the influence of conformational dynamics on the ROA patterns of  $\alpha$ -helical structure was investigated. In **Figure 2**, the spectra of the HCO-(Ala)<sub>7</sub>-NH<sub>2</sub> model peptide in an  $\alpha$ -helical conformation with typical backbone torsion angles  $\phi = -66^\circ$  and  $\psi = -41^\circ$  is shown and how the Raman and ROA patterns are affected when these specific torsion angles are increasingly randomized. As shown in **Figure 2 (a)** and **(b)**, with high standard deviations  $\sigma$  of the mean  $\phi$  and  $\psi$  angles, the regular  $\alpha$ -helical structure is very much randomized from the regular conformation. Because of that, both the Raman and ROA spectra of the individual conformations in each family are strongly affected as shown in the superimposed spectra in **Figure 2 (c)**. It is therefore a striking result that the mean spectra of each family of conformations are so similar (see **Figure 2 (d)**). The largest spectral differences in the mean spectra are observed in the lower wavenumber region that drops significantly in maximal intensities and in the amide I region, which loses the negative portion of the characteristic  $-/+$  couplet. As we showed before that the amide III region is very sensitive to the exact  $\alpha$ -helical conformation,<sup>10</sup> it is a remarkable result that the mean patterns here are so similar. While the individual spectra shown in **Figure 2 (c)** show a lot of variation in that region, the mean spectra show the same relative intensities of the  $-/+$  pattern.

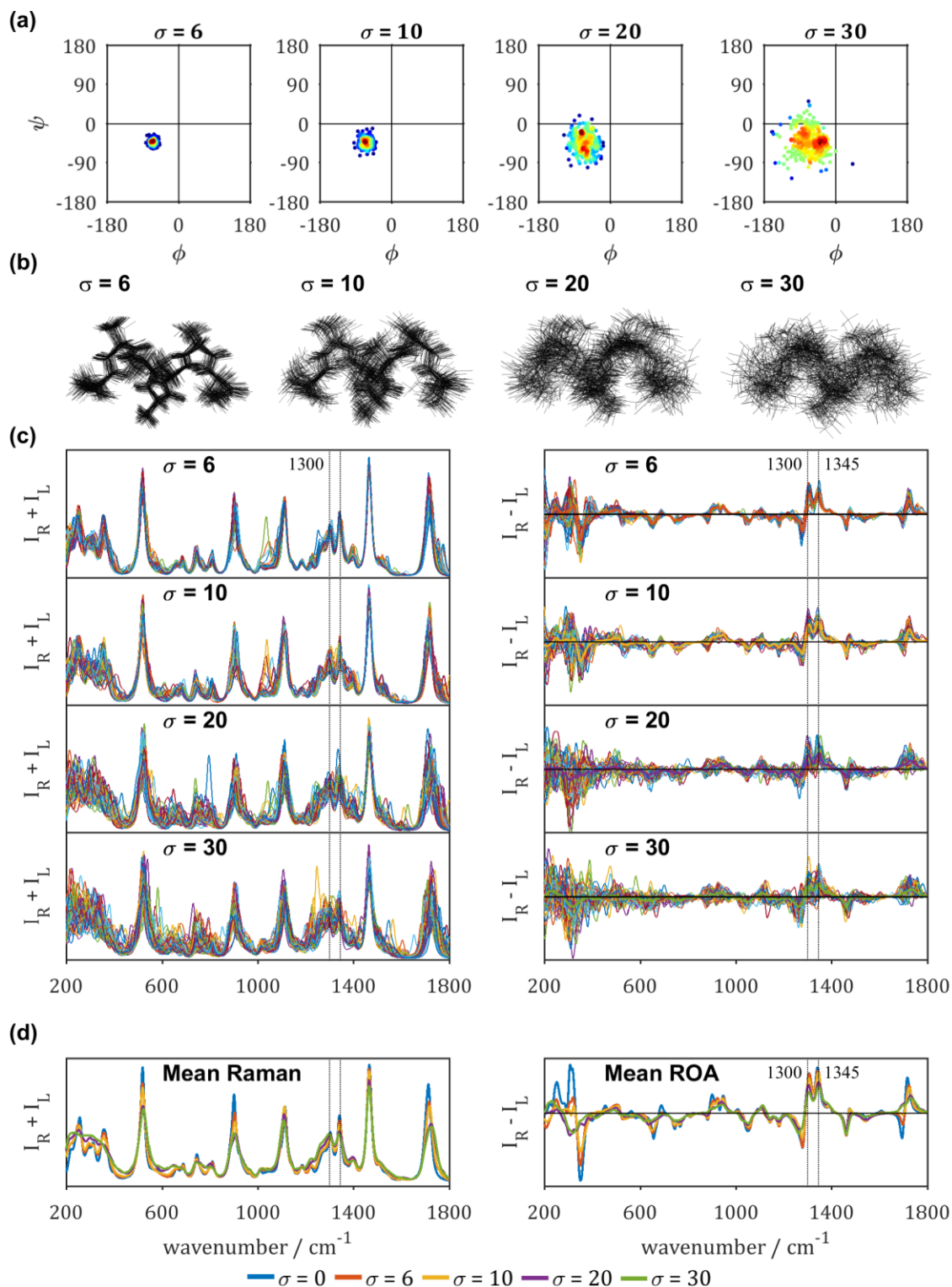


**Figure 2.** Effect of conformational disorder on the ROA patterns of  $\alpha$ -helical secondary structure. The backbone conformation of  $\text{HCO}(\text{L-Ala})_7\text{-NH}_2$  is increasingly randomized by

deviating each  $\phi$  and  $\psi$  angle in the backbone from  $\phi = -66^\circ$  and  $\psi = -41^\circ$  to  $\phi = -66^\circ \pm \sigma$  and  $\psi = -41^\circ \pm \sigma$ . (a) Ramachandran plots displaying the increasing deviation from the central  $\phi = -66^\circ$  and  $\psi = -41^\circ$  angles for each family of 50 structures with a set standard deviation  $\sigma$ . (b) Superposition of the 50 conformations of HCO-(L-Ala)<sub>7</sub>-NH<sub>2</sub> shown as stick figures for each conformational family. The y-axis is set to the same limits. (c) Individual Raman ( $I_R+I_L$ ) and ROA ( $I_R-I_L$ ) spectra of each family of 50 conformations. (d) Mean Raman and ROA spectra of the four families ( $\sigma = 6$  (red), 10 (yellow), 20 (purple) or 30 (green)) compared to the computed spectrum of HCO-(L-Ala)<sub>7</sub>-NH<sub>2</sub> with all backbone angles set to  $\phi = -75^\circ$  and  $\psi = 145^\circ$  (blue;  $\sigma = 0$ ).

### **ROA is sensitive to the mean $\alpha$ -helical conformation.**

As our previous work showed that ROA is very sensitive to the exact  $\alpha$ -helical conformation,<sup>10</sup> the results shown in **Figure 2** were extended to other  $\alpha$ -helical conformations (specific pairs of  $\phi$  and  $\psi$  angles) to study the effect of conformational disorder in more detail. Similar to the results discussed above, firstly the ROA spectra of regular HCO-Ala<sub>7</sub>-NH<sub>2</sub> model conformations with repeated  $\phi$  and  $\psi$  backbone angles were computed. These computed Raman and ROA spectra are shown in **Figure 3** by the blue lines and thus correspond to a Raman and a ROA spectrum of a single conformation. By looking at five different pairs of  $\phi$  and  $\psi$  angles, the effect of slight differences in the  $\alpha$ -helical conformation is evaluated. These results are also compared to a  $3_{10}$ -helical conformation ( $\phi = -71^\circ$  and  $\psi = -18^\circ$ ) to confirm the structural sensitivity of ROA to different types of helix. The red, yellow, purple and green lines correspond to the average spectra of families of 50 structures with the standard deviation  $\sigma$  of the mean  $\phi$  and  $\psi$  backbone

angles being  $\sigma = 6, 10, 20$  or  $30$ , respectively (see **Figure S1-S5** for the spectra of the individual conformations).

The mean Raman spectra in **Figure 3** mostly show broadening of the spectral patterns with increasing conformational disorder (higher  $\sigma$ ) from the original regular helix conformation (blue;  $\sigma = 0$ ). The spectral differences in the mean ROA spectra are similar to those observed in **Figure 2**. Also for the other  $\alpha$ -helical conformations, the amide I region in the ROA spectra in **Figure 3** does not show the negative contribution of the couplet upon increasing conformational disorder. Since for  $\alpha$ -helical proteins and peptides the amide I is always observed as a  $-/+$  couplet, this indicates that this spectral pattern arises from regular helical structure with a limited variation of the backbone  $\varphi$  and  $\psi$  angles.

In accordance with our previous analysis,<sup>10</sup> the spectra of the  $\alpha$ -helical models with slightly different mean backbone angles show markedly different amide III patterns. This is observed in **Figure 3**, by comparing the ROA spectra of the same color. For example, the blue spectra of the top three panels show a much higher positive maximum intensity around  $1345\text{ cm}^{-1}$ , relative to the  $1300\text{ cm}^{-1}$  band, compared to the ratio in the panels below.

The effect of increasingly deviating the conformation from the regular conformation can be seen by comparing the ROA spectra within the same panel from  $\sigma = 0$  (blue) to  $\sigma = 30$  (green). Very surprisingly, the amide III region of the  $\alpha$ -helical models is robust with the increase in variation of the backbone conformation; in other words, the  $-/+$  pattern and relative ratios remain generally the same for each combination of  $\varphi$  and  $\psi$  angles. This shows that the amide III region of  $\alpha$ -helical proteins is a pattern resulting from the average helix conformation in the structural ensemble. In agreement with our previous results, the positive band around  $1345\text{ cm}^{-1}$  is a robust marker of  $\alpha$ -helical structure; it is found in all calculated spectra of  $\alpha$ -helical structure,

even if the helix is considerably random (see spectra for  $\sigma = 20$  or  $30$ ). The positive band around  $1300\text{ cm}^{-1}$  is very sensitive to the combination of  $\phi$  and  $\psi$  angles and has a very low (even negative) value for structures with backbone angles in the bottom right of the  $\alpha$ -helical region of the Ramachandran plot and gradually increases for structures with backbone angles towards the top left of the  $\alpha$ -helical region (see **Figure 3** and ref <sup>10</sup>).

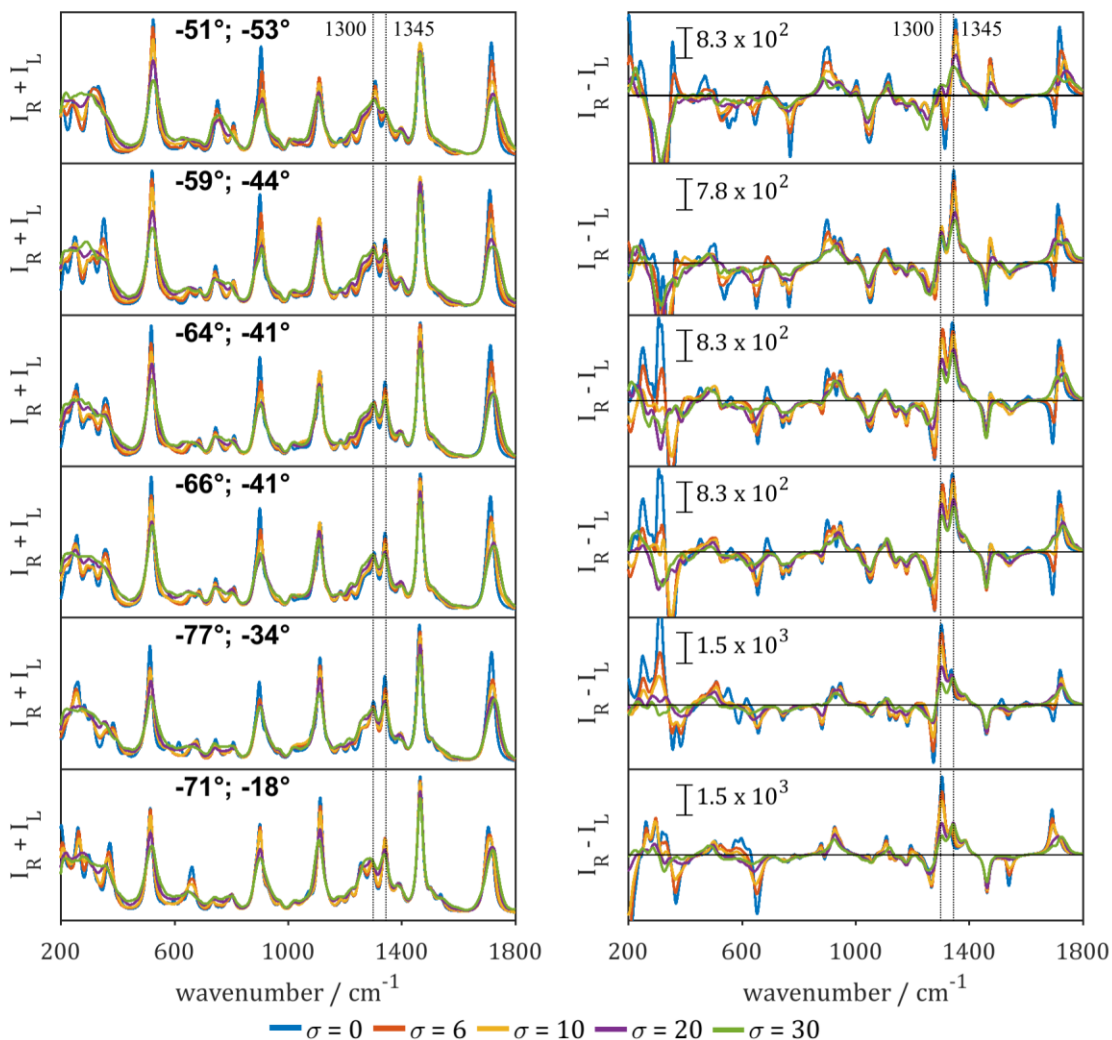


**Figure 3.** Effect of conformational disorder on the ROA patterns of left-handed helical secondary structure. For six couples of  $\phi$  and  $\psi$  angles, the conformation of  $\text{HCO-(L-Ala)}_7\text{-NH}_2$  was increasingly randomized by deviating each  $\phi$  and  $\psi$  angle in the backbone from the initial  $\phi$

and  $\psi$  to  $\phi \pm \sigma$  and  $\psi \pm \sigma$  in families of 50 conformations with respective standard deviation  $\sigma$ . Mean Raman ( $I_R+I_L$ ) and ROA ( $I_R-I_L$ ) spectra of HCO-Ala<sub>7</sub>-NH<sub>2</sub> with backbone torsion angles set to various values corresponding to  $\alpha$ -helical secondary structure or  $3_{10}$ -helix ( $\sigma = 0$ ; blue) and the deviation from that with torsion angles with a standard deviation from these angles set to  $\sigma = 6$  (red), 10 (yellow), 20 (purple) or 30 (green). The red, yellow, purple and green spectra correspond to the average of 50 spectra of the family of 50 model structures with randomly generated normal distributed torsion angles.

These observations are further supported by analyzing the ratio of the maximum intensity of the two positive bands at 1300 cm<sup>-1</sup> and 1345 cm<sup>-1</sup> in the amide III region in **Figure 4**. In accordance with our earlier results, the ratio is very sensitive to the exact combination of the  $\phi$  and  $\psi$  angles, observing very high ratios for structures with backbone angles in the top left of the helical region in the Ramachandran plot, to much lower ratios in the bottom right. Both for the  $\alpha$ -helical model with torsion angles set  $\phi = -77^\circ$  and  $\psi = -34^\circ$  and the  $3_{10}$ -model with  $\phi = -71^\circ$  and  $\psi = -18^\circ$ , the positive band around 1300 cm<sup>-1</sup> has a very high intensity that collapses with increasing conformational freedom.

Only with a very high degree of conformational dynamics or disorder ( $\sigma = 30$ ), all helical models, including the  $3_{10}$ -conformation, obtain a similar ROA pattern (**Figure 3**) and intensity ratio (**Figure 4**). To conclude the above results, the intensity ratio of the two bands is sensitive to the average helical conformation.



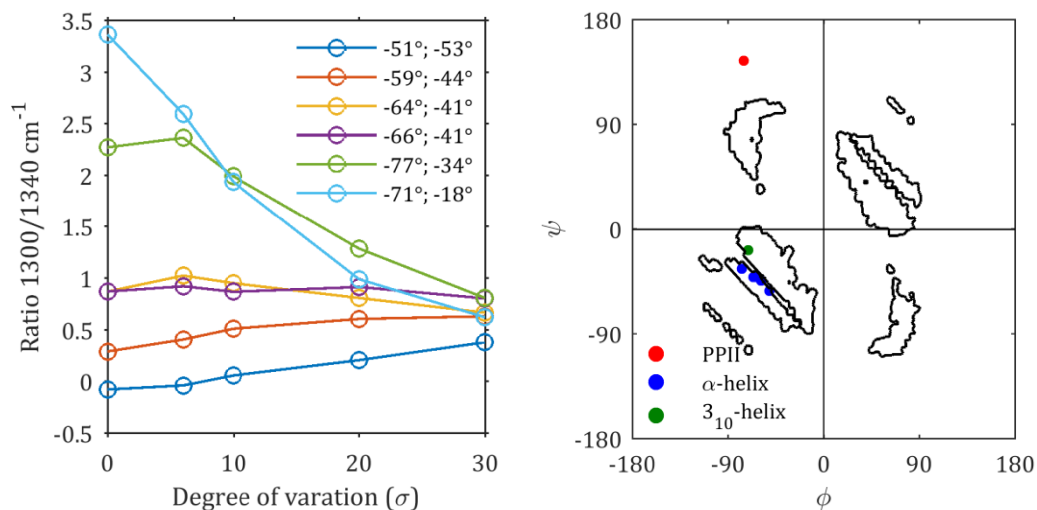


**Figure 4.** (Left) Ratio of the maximum intensity of the two positive bands in the extended amide III region of the ROA spectrum at 1300/1345 cm<sup>-1</sup>. (right) Ramachandran plot showing the (φ;ψ) pairs of angles used in this study (right): (-75°;145°), (-51°;-53°), (-59°;-44°), (-64°;-41°), (-66°;-41°), (-77°;-34°), (-71°;-18°). The contour lines mark different secondary structure regions based on the hydrogen bonding in regular model alanine peptides (see ref<sup>10</sup>).

### The effect of mixing PPII with other secondary structures on the ROA patterns

As discussed above, IDPs adopt a substantial amount of PPII in their structural ensembles. The results discussed above furthermore showed that the experimental ROA patterns do not agree with very flexible chains with average torsion angles around PPII angles (φ = -75° and ψ = 145°). More likely, short stretches of PPII with average angles close to φ = -75° and ψ = 145° but truncated by other secondary structure elements fit better with experiment.

To further study the ROA patterns associated with IDPs, here the effect of PPII mixing with other secondary structure components is therefore explored. First, the behavior in solution of IDPs is considered. The protein α-synuclein, for example, has received an extensive amount of scientific interest due to its central involvement in Parkinson's disease and related neurodegenerative diseases (termed synucleinopathies).<sup>7,25,26</sup> Our group reported the

experimental ROA patterns of  $\alpha$ -synuclein adopting different conformations, yet, the origin of the spectral patterns of IDPs and small differences in their ROA spectra are unknown.<sup>7</sup> To describe the flexible structure of IDPs, multiple structural ensembles have been proposed based on NMR approaches. In **Figure 5**, the Ramachandran plots of three of such structural ensembles of  $\alpha$ -synuclein are shown. All three display distinct conformational preferences.

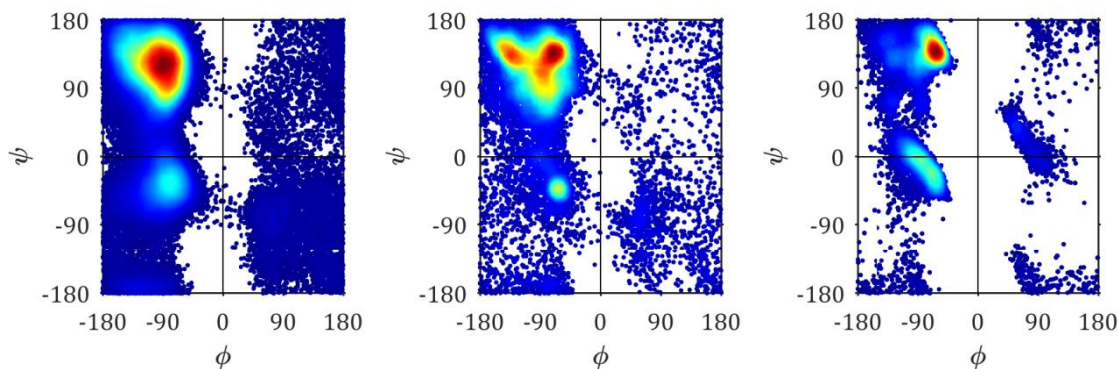


**Figure 5.** Ramachandran plots of the  $\alpha$ -synuclein ensembles by Allison *et al.* (left), Tóth *et al.* (middle) and Schwalbe *et al.* <sup>25–27</sup>

Due to differences in the methodology of these three studies, the Ramachandran plots of the ensembles are quite different. Yet, all three of the graphs show that most backbone torsion angles fluctuate in the PPII region, while the left-handed helical region is also populated. The ensemble by Tóth *et al.* (middle) furthermore shows an important contribution of the  $\beta$ -strand region. Based on these graphs, the mixing of PPII structure with either helical or  $\beta$ -strand structure was explored. To this end, the Raman and ROA spectra of HCO-Ala<sub>7</sub>-NH<sub>2</sub> model peptides that differ in the ratio of PPII/helix or PPII/ $\beta$ -strand were computed. As before, families of 50 structures were created by defining the backbone torsion angles. To include conformational freedom in these families of structures, a standard deviation of the mean backbone angles of  $\sigma = 20$  was used. Next, ensembles of 50 structures with different specified ratios of PPII/helix or PPII/ $\beta$ -strand were generated as visualized in the Ramachandran plots in **Figure 6** and **Figure 7**.

In **Figure 6**, the average ROA spectra of the different conformational families of PPII/helix are shown (the corresponding Raman spectra are shown in **Figure S6**). The amide I band in both the Raman and ROA shifts down about  $15\text{ cm}^{-1}$  going from 100 % PPII to 100 % left-handed helix, because of the presence of  $\text{C}=\text{O}\cdots\text{H}-\text{N}$  hydrogen bonds in the helical structures. A broad amide III band around  $1230\text{-}1240\text{ cm}^{-1}$  in the Raman spectra, gradually decreases, marking the reduction in PPII content while the positive bands around  $1300\text{ cm}^{-1}$  and  $1345\text{ cm}^{-1}$  increase, both arising from  $\text{C}\alpha\text{-H}$  bending modes coupled to amide III vibrational motions in helical structure.

In the ROA spectra, the change in the extended amide III region is more visible with the positive band at  $1318\text{ cm}^{-1}$  (100% PPII) becoming broader upon increase in helical content, with eventually the appearance of the characteristic two positive bands marking  $\alpha$ -helical structure around  $1300\text{ cm}^{-1}$  and  $1345\text{ cm}^{-1}$  (100% helix). Two important conclusions can be drawn from this graph. First, the broad asymmetric band in the amide III region in the ROA spectra with mixed PPII/helix suggests that the extended amide III region in experimental ROA spectra of IDPs arises from PPII segments mixed with other structural elements such as helical structure. Second, the appearance of the two positive ROA bands marking  $\alpha$ -helical structure at  $1300\text{ cm}^{-1}$  and  $1345\text{ cm}^{-1}$  only for a content of 80-100 % helix again shows that ROA is sensitive to rigid secondary structure elements in solution. As experimental ROA spectra of proteins in solution with much less helical content than 80 % already show the two positive bands, these bands must arise from sequences of multiple residues adopting a left-handed helix. Since here a helix with  $3_{10}$ -backbone angles was considered, the unfolding of an  $\alpha$ -helix to PPII structure was calculated to further study the mixing of secondary structures.

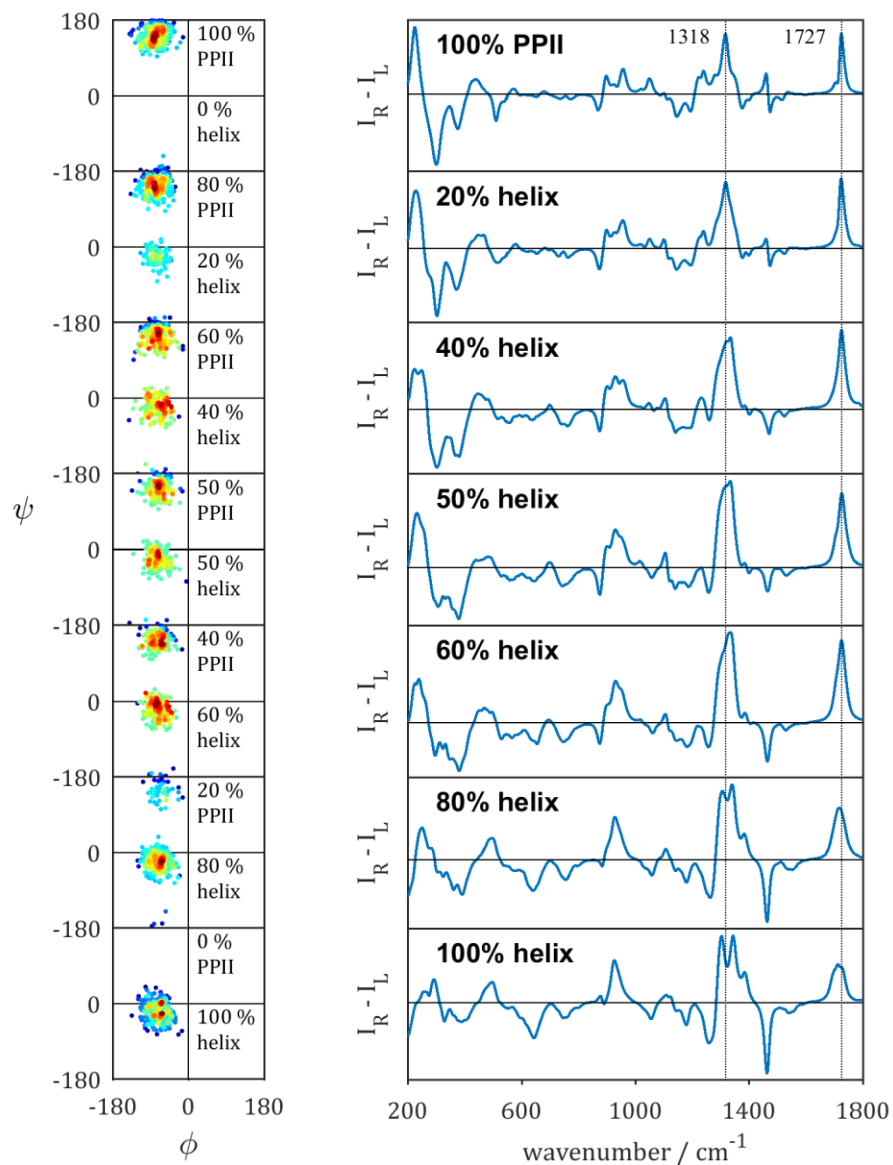


**Figure 6.** Mixing of PPII with left-handed helical structure: Ramachandran plots of the backbone angles of each family of 50 DFT optimized structures with a specific ratio of PPII/helix. For PPII ( $-75^\circ$ ;  $145^\circ$ ) was used as the central pair of angles and for the helical structures ( $-71^\circ$ ;  $-18^\circ$ ) (see Ramachandran plot for the ensemble by Schwalbe *et al.* in **Figure 5**). On the right-hand side the ROA ( $I_R - I_L$ ) spectra are shown as the average of 50 spectra of 50 structures.

As the Ramachandran plot of the ensemble of  $\alpha$ -synculein by Tóth *et al.* shows an important population of the  $\beta$ -strand region (**Figure 5**), the effect of the mixing of PPII with  $\beta$ -strand structure on the ROA patterns was also probed here. Similar to the previous calculations, multiple families of 50 structures with different ratios of PPII/ $\beta$ -strand were generated (see the Ramachandran plot in **Figure 7**). As can be seen in the computed spectra of these conformational families, the amide I region is not much shifted upon variation of the PPII/ $\beta$ -strand ratio (the corresponding Raman spectra are shown in **Figure S7**). However, as can be seen in **Figure 7**, the ROA amide I does change shape quite distinctly, with a negative band emerging upon increase in the  $\beta$ -strand content. This spectral change hence arises from the change in the orientation of the C=O groups and not from hydrogen bonding.

The extended amide III region is quite sensitive to the mixing of PPII/ $\beta$ -strand in both the Raman and ROA spectra. A positive amide III band appears around  $1240\text{ cm}^{-1}$  in the ROA spectra upon increasing the  $\beta$ -strand content, as well as a broad negative band in the region  $1345\text{--}1370\text{ cm}^{-1}$ . The experimental ROA spectrum of for example poly-L-lysine in  $\beta$ -sheet state, displays a broad positive band around  $1260\text{ cm}^{-1}$  and a negative band at  $1351\text{ cm}^{-1}$ .<sup>28</sup> Such a negative band is often observed in the experimental ROA spectra of proteins with a large  $\beta$ -sheet content.<sup>28</sup> While for the mixing of PPII with helical structure the skeletal stretch region changed from a typical PPII -/+ signature ( $860\text{--}980\text{ cm}^{-1}$ ) to a positive band ( $930\text{ cm}^{-1}$ ) with high helical content, this spectral pattern -/+ ( $860\text{--}980\text{ cm}^{-1}$ ) upon mixing PPII with  $\beta$ -strand structure remains the same.

To conclude, the spectral features that appear in the ROA spectra in **Figure 7** upon increasing the  $\beta$ -strand content, do not reflect spectral patterns observed experimentally for IDPs. The ROA

spectra of mixing PPII backbone torsion angles with helical backbone torsion angles is on the other hand reminiscent of the experimental ROA spectral patterns observed for IDPs. Finally, to further study the mixing of PPII with helical secondary structure, in the next section the unfolding of an  $\alpha$ -helix to a PPII backbone is studied.

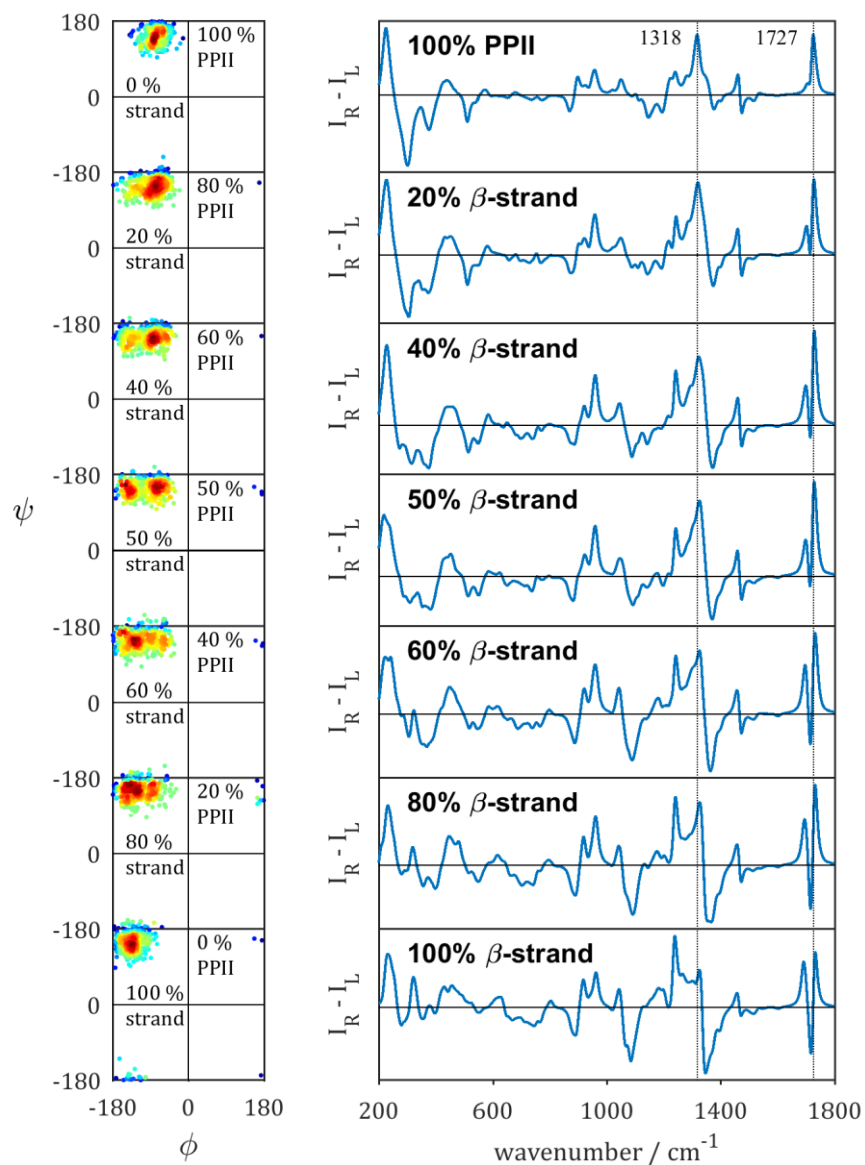


**Figure 7.** Mixing of PPII with  $\beta$ -strand structure: Ramachandran plots of the backbone angles of each family of 50 DFT optimized conformations with a specific ratio of PPII/helix. For PPII (-75°; 145°) was used as the central angles and for the  $\beta$ -strand: (-125°; 150°) (see Ramachandran

plot for the Tóth ensemble in **Figure 5**). On the right-hand side the ROA ( $I_R - I_L$ ) spectra are shown as the average of 50 spectra of the 50 corresponding structures.

### **$\alpha$ -Helix unfolding to PPII**

Above, the transition of helical structure to PPII secondary structure was probed by varying all backbone torsion angles of a peptide model simultaneously and calculating the Raman and ROA spectra at set percentages of the two secondary structures (two pairs of  $\phi$  and  $\psi$  angles). In this section, the change in the spectra is considered when one regular  $\alpha$ -helical model peptide makes a gradual transition to PPII extended helix by changing the backbone angles of each residue one by one starting from the N-terminus. By doing this for a  $\text{HCO}-(\text{L-Ala})_{11}-\text{NH}_2$  peptide, the difference with the results described above, is that multiple consecutive residues of both secondary structure types coexist within the same peptide.

As shown in **Figure 8**, upon varying the structure from 100 % PPII to 100 %  $\alpha$ -helix, the largest changes in the Raman spectra appear in the regions  $500\text{-}550\text{ cm}^{-1}$  (backbone deformations and out-of-plane N-H bending), the extended amide III region and the amide I region. The ROA spectra show considerable changes across the entire spectral window. The amide I in the ROA spectra changes from a positive band associated with PPII structure to a  $-/+$  couplet marking  $\alpha$ -helical structure. The most interesting spectral region appears to be the amide III region that retains a strong positive band around  $1300\text{-}1325\text{ cm}^{-1}$ , while only for the spectrum consisting of 100 %  $\alpha$ -helical backbone the two positive amide III bands are clearly distinguishable.

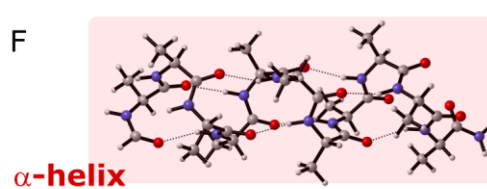
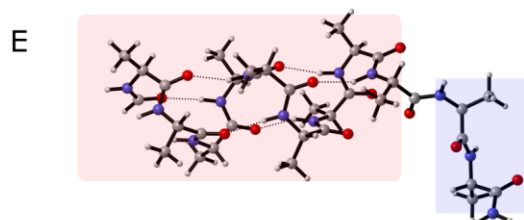
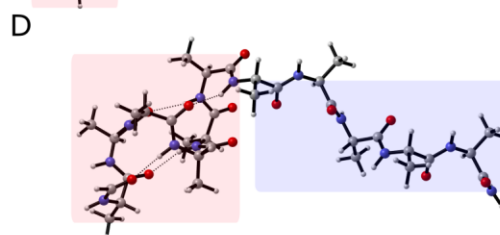
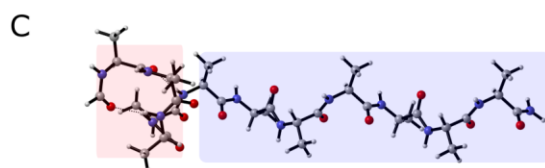
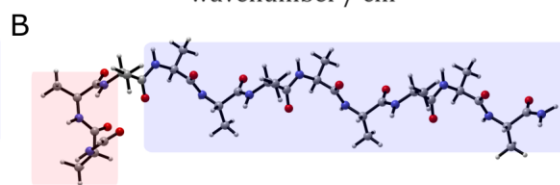
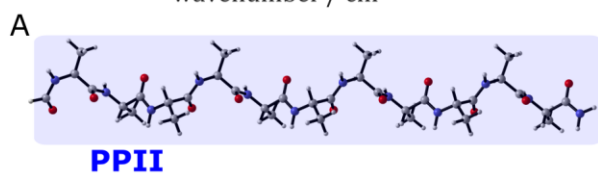
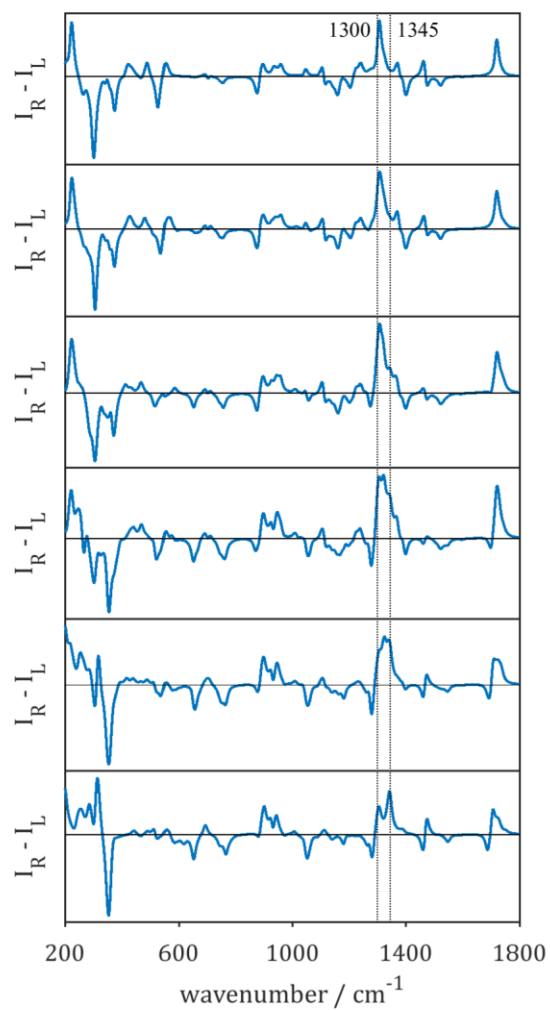
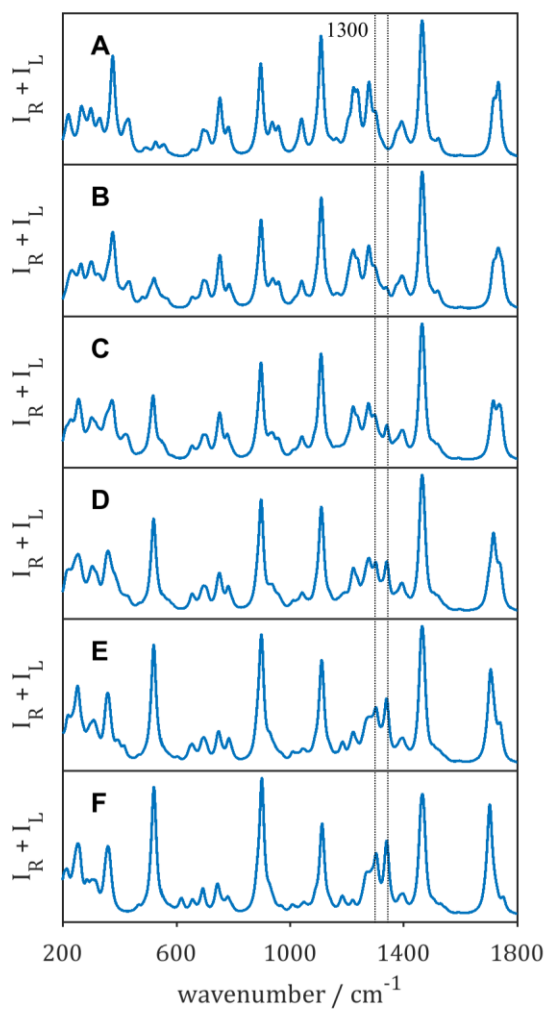




**Figure 8.** Raman ( $I_R+I_L$ ) and ROA ( $I_R+I_L$ ) spectra of an  $\alpha$ -helix unfolding to PPII conformation starting from the N-terminus. Each spectrum is calculated for a HCO-Ala<sub>11</sub>-NH<sub>2</sub> model peptide. From A-F, each time the next two consecutive ( $\phi$ ;  $\psi$ ) angles are changed from (75°; 145°) to (-64°; 41°).

In **Figure 9**, the amide III spectral region is shown in more detail. There are different contributions to the extended amide III region. The vibrational modes in this spectral region arise from the coupling of C-N stretching with C $\alpha$ -H and N-H bending. In the lower half of the region (below 1300 cm<sup>-1</sup>) the C-N stretching is dominant, while in the higher wavenumber region 1300-1400 cm<sup>-1</sup>, C-H and N-H bending have a higher contribution to the complex amide III modes.<sup>24</sup> The coupling of the latter two bending modes is very sensitive to the exact geometry and is considered one of the most important regions in the ROA spectrum due to the intense bands ~ 1230-1350 cm<sup>-1</sup>.<sup>1</sup> In **Figure 9**, with higher  $\alpha$ -helical content in the model peptide, a negative amide III band appears below 1300 cm<sup>-1</sup>. Furthermore, four positive bands are observed in the C $\alpha$ -H bending mode region (1300-1370 cm<sup>-1</sup>). PPII structure has a prominent positive band at 1308 cm<sup>-1</sup> that diminishes with increasing  $\alpha$ -helical content. The shoulder around 1323 cm<sup>-1</sup> becomes more evident for the mixed PPII/ $\alpha$ -helical structures. Only for the fully  $\alpha$ -helical model structure, the ROA band marking  $\alpha$ -helical structure at 1343 cm<sup>-1</sup> is separately observed without the band around 1323 cm<sup>-1</sup>. The band around 1323 cm<sup>-1</sup> has two important contributions: firstly amide III modes in the backbone and secondly an amide III mode of the C-terminus. The latter mode arising from the capping of the peptide model possibly explains the intense appearance of the band in the amide III region of the mixed PPII/ $\alpha$ -helix structures. A fourth C $\alpha$ -H bending mode band is observed around 1370 cm<sup>-1</sup> for the structures with a high PPII content.

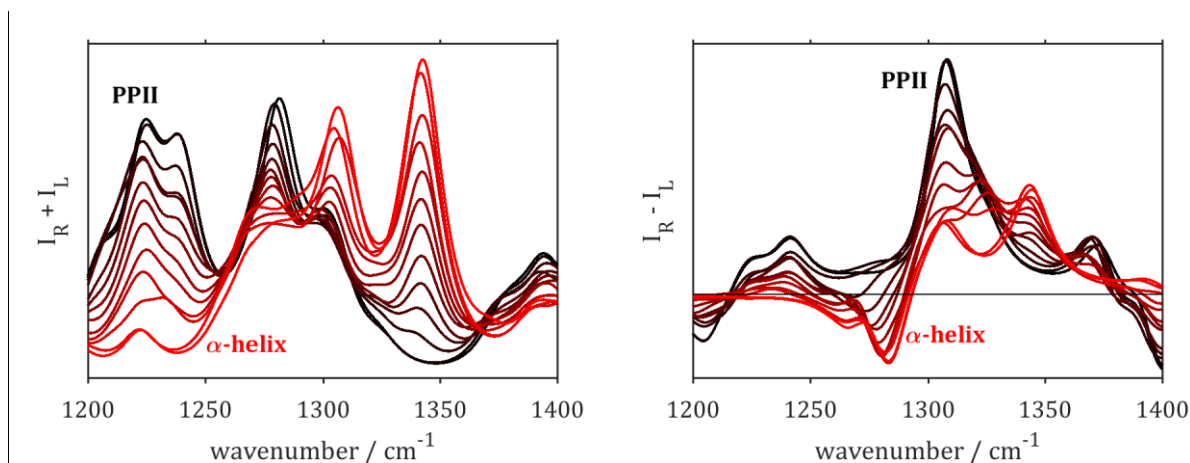


**Figure 9.** Raman ( $I_R + I_L$ ) and ROA ( $I_R - I_L$ ) spectra in the extended amide III region of HCO-(L-Ala)<sub>11</sub>-NH<sub>2</sub> in an  $\alpha$ -helical conformation (red) that was unfolded to a PPII backbone conformation starting from the N-terminus to an  $\alpha$ -helix (red). Ranging from the red to the black colored lines, one pair of consecutive ( $\phi$ ;  $\psi$ ) angles is for each consecutive spectrum changed from (75°; 145°) to (-64°; 41°).

A few conclusions can be drawn from **Figure 9**. First, the amide III band around 1340-1345 cm<sup>-1</sup> is the most reliable marker for  $\alpha$ -helical structure. Even for a minor contribution of  $\phi$  and  $\psi$   $\alpha$ -helical angles, this band is observed. It mainly arises from C $\alpha$ -H bending with its motion parallel to the C $\alpha$ -N bond. The diminishing of this ROA band around 1345 cm<sup>-1</sup> is reminiscent of the gradual disappearing of that band in the experimental ROA spectra of thermally unfolding  $\alpha$ -lactalbumin.<sup>29,30</sup> On the other hand, positive intensity in the ROA around 1300-1310 cm<sup>-1</sup> is witnessed both for  $\alpha$ -helical and PPII secondary structure here, and should hence be carefully assigned. Furthermore, the region 1200-1300 cm<sup>-1</sup> has an important contribution from C-N stretching, which is very dependent to hydrogen bonding, e.g. with water.<sup>31</sup> For structures with a large content of PPII structure, intense Raman bands are observed in that region in **Figure 9**. However, PPII structure is not stabilized by intramolecular hydrogen bonds such as is the case in  $\alpha$ -helical structure, rather the carbonyl groups pointing outwards from the backbone allow

hydrogen bonding with water.<sup>11</sup> This urges the need to study the effect of explicit hydration on the ROA patterns in more detail, specifically in the case of PPII structure. Also the negative ROA band around 1280 cm<sup>-1</sup> appears upon hydrogen bond formation in the  $\alpha$ -helical segment of the model peptide. Experimentally, the ROA spectra of IDPs show a negative band in this region. Based on the calculations in this study, there are no indications this negative band arises from PPII secondary structure, which is the main structural element of IDPs. The calculated spectra in this study however show that it could arise from helical contributions.

## Conclusions

This study of the effect of conformational dynamics and structural disorder showed that ROA patterns mainly reflect the average distribution of the backbone conformation. Therefore, the approach to elucidate experimental ROA spectra based on a large database of calculated spectra of fixed model structures reported before by our group is a good simple methodology to study the amide modes.<sup>10</sup> Only upon larger variation of the backbone angles of common secondary structure elements such as PPII and left-handed helical structure, the ROA patterns average.

This study furthermore supports the view that experimental ROA patterns likely stem from the most rigid components in the structural ensemble. For example, in the case of IDPs, a strong positive band  $\sim 1318$  cm<sup>-1</sup> in the amide III reflects PPII secondary structure with backbone angles close (variation of the mean angles  $\sigma \leq 20^\circ$ ) to the average PPII backbone angles ( $\phi = -75^\circ$  and  $\psi = 145^\circ$ ), rather than a fully flexible structure with the mean backbone angles being  $\phi = -75^\circ$  and  $\psi = 145^\circ$ . Furthermore, the mixing of PPII with other secondary structure elements may explain the experimentally observed ROA patterns. Mixing of PPII structure with right-handed helical structure is more reminiscent of experimental ROA patterns than mixing with  $\beta$ -strand

structure. Both hydration<sup>32</sup> and the explicit side-chains<sup>33,34</sup> have been suggested to influence the ROA patterns, yet these effects are not fully understood. Future research on the ROA patterns of proteins should therefore focus on the effect of explicit solvation and the effect of the amino acid side-chains on the on the calculated spectra. Since IDPs are hydrated, the effect of water molecules near the peptide will probably have a large effect on the amide modes. Furthermore, it was shown that ROA is extremely sensitive to the exact conformation of  $\alpha$ -helical structure and the tilt of the carbonyl groups in the C=O $\cdots$ H-N hydrogen bonds, which could be affected by explicit hydrogen bonding with water.<sup>10</sup> Also the CH and CH<sub>2</sub> groups in amino acid side-chains could have a pronounced effect on e.g. the amide III region through coupling of the vibrational modes of these groups with C $\alpha$ -H and N-H bending modes, which will hence be the focus of our future research.

## ASSOCIATED CONTENT

### **Supporting Information.**

The Raman and ROA spectra of the separate conformations of which the mean spectra are shown in Figure 3 as well as the Raman spectra computed for the conformations for which to the ROA spectra are shown in Figure 6 and Figure 7 are included in the supporting information. This material is available free of charge online at <http://pubs.acs.org/>.

## AUTHOR INFORMATION

### **Corresponding Author**

\*Phone: +32 3 265 35 05. Fax: +32 3 265 32 33. E-mail: [christian.johannessen@uantwerpen.be](mailto:christian.johannessen@uantwerpen.be).

## ACKNOWLEDGMENT

We thank the Flemish Supercomputing Centre (VSC) for providing computing resources and support. C.M. acknowledges the University of Antwerp for funding his research. C.M. also thanks prof. Malene Ringkjøbing Jensen and prof. Michele Vendruscolo for providing the  $\alpha$ -synuclein ensembles.

## ABBREVIATIONS

ROA, Raman optical activity; IDP, intrinsically disordered protein; DFT, density functional theory; PPII, poly-L-proline type II helix; NMR, nuclear magnetic resonance; scrf, self-consistent reaction field.

## REFERENCES

- (1) Barron, L. D.; Hecht, L.; Blanch, E. W.; Bell, A. F. *Prog. Biophys. Mol. Biol.* **2000**, *73*, 1–49.
- (2) Barron, L. D. *Biomed. Spectrosc. Imaging* **2015**, *4*, 223–253.
- (3) Hudecová, J.; Kapitán, J.; Baumruk, V.; Hammer, R. P.; Keiderling, T. A.; Bouř, P. *J. Phys. Chem. A* **2010**, *114*, 7642–7651.
- (4) Mensch, C.; Pendrill, R.; Widmalm, G.; Johannessen, C. *ChemPhysChem* **2014**, *15*, 2252–2254.
- (5) Johannessen, C.; Pendrill, R.; Widmalm, G.; Hecht, L.; Barron, L. D. *Angew. Chemie Int. Ed.* **2011**, *50*, 5349–5351.
- (6) Van de Vondel, E.; Mensch, C.; Johannessen, C. *J. Phys. Chem. B* **2016**, *120*, 886–890.
- (7) Mensch, C.; Konijnenberg, A.; Van Elzen, R.; Lambeir, A.-M.; Sobott, F.; Johannessen, C. *J. Raman Spectrosc.* **2017**, *48*, 910–918.

- (8) Uversky, V. N. *Protein Sci.* **2013**, 22, 693–724.
- (9) Wilson, G.; Hecht, L.; Barron, L. D. *Biochemistry* **1996**, 35, 12518–12525.
- (10) Mensch, C.; Barron, L. D.; Johannessen, C. *Phys. Chem. Chem. Phys.* **2016**, 18, 31757–31768.
- (11) Adzhubei, A. A.; Sternberg, M. J. E.; Makarov, A. A. *J. Mol. Biol.* **2013**, 425, 2100–2132.
- (12) Tien, M. Z.; Sydykova, D. K.; Meyer, A. G.; Wilke, C. O. *PeerJ* **2013**, 1, e80.
- (13) Bouř, P.; Keiderling, T. A. *J. Chem. Phys.* **2002**, 117, 4126–4132.
- (14) Frisch, M. J.; Trucks, G. W.; Schlegel, H. B.; Scuseria, G. E.; Robb, M. A.; Cheeseman, J. R.; Scalmani, G.; Barone, V.; Petersson, G. A.; Nakatsuji, H.; Li, X.; Caricato, M.; Marenich, A. V.; Bloino, J.; Janesko, B. G.; Gomperts, R.; Mennucci, B.; Hratchian, H. P.; Ortiz, J. V.; Izmaylov, A. F.; Sonnenberg, J. L.; Williams-Young, D.; Ding, F.; Lipparini, F.; Egidi, F.; Goings, J.; Peng, B.; Petrone, A.; Henderson, T.; Ranasinghe, D.; Zakrzewski, V. G.; Gao, J.; Rega, N.; Zheng, G.; Liang, W.; Hada, M.; Ehara, M.; Toyota, K.; Fukuda, R.; Hasegawa, J.; Ishida, M.; Nakajima, T.; Honda, Y.; Kitao, O.; Nakai, H.; Vreven, T.; Throssell, K., Jr., J. A. M.; Peralta, J. E.; Ogliaro, F.; Bearpark, M. J.; Heyd, J. J.; Brothers, E. N.; Kudin, K. N.; Staroverov, V. N.; Keith, T. A.; Kobayashi, R.; Normand, J.; Raghavachari, K.; Rendell, A. P.; Burant, J. C.; Iyengar, S. S.; Tomasi, J.; Cossi, M.; Millam, J. M.; Klene, M.; Adamo, C.; Cammi, R.; Ochterski, J. W.; Martin, R. L.; Morokuma, K.; Farkas, O.; Foresman, J. B.; Fox, D. J. Gaussian 16, Revision A.03, 2016.
- (15) Jmol: an open-source Java viewer for chemical structures in 3D. <http://www.jmol.org/>.

- (16) CYLview: Visualization and analysis software for computational chemistry.  
<http://www.cylview.org/>.
- (17) Barron, L. D.; Zhu, F.; Hecht, L.; Tranter, G. E.; Isaacs, N. W. *J. Mol. Struct.* **2007**, *834–836*, 7–16.
- (18) Zhu, F.; Kapitan, J.; Tranter, G. E.; Pudney, P. D. A.; Isaacs, N. W.; Hecht, L.; Barron, L. D. *Proteins Struct. Funct. Bioinforma.* **2007**, *70*, 823–833.
- (19) Blanch, E. W.; Morozova-Roche, L. A.; Cochran, D. A. E.; Doig, A. J.; Hecht, L.; Barron, L. D. *J. Mol. Biol.* **2000**, *301*, 553–563.
- (20) Schweitzer-Stenner, R.; Measey, T. J. *Proc. Natl. Acad. Sci.* **2007**, *104*, 6649–6654.
- (21) Zagrovic, B.; Lipfert, J.; Sorin, E. J.; Millett, I. S.; van Gunsteren, W. F.; Doniach, S.; Pande, V. S. *Proc. Natl. Acad. Sci.* **2005**, *102*, 11698–11703.
- (22) Blanch, E. W.; Bell, A. F.; Hecht, L.; Day, L. A.; Barron, L. D. *J. Mol. Biol.* **1999**, *290*, 1–7.
- (23) Blanch, E. W.; Hecht, L.; Day, L. A.; Pederson, D. M.; Barron, L. D. *J. Am. Chem. Soc.* **2001**, *123*, 4863–4864.
- (24) Jacob, C. R.; Reiher, M. *J. Chem. Phys.* **2009**, *130*, 084106.
- (25) Tóth, G.; Gardai, S. J.; Zago, W.; Bertoncini, C. W.; Cremades, N.; Roy, S. L.; Tambe, M. A.; Rochet, J.-C.; Galvagnion, C.; Skibinski, G.; Finkbeiner, S.; Bova, M.; Regnstrom, K.; Chiou, S.-S.; Johnston, J.; Callaway, K.; Anderson, J. P.; Jobling, M. F.; Buell, A. K.; Yednock, T. A.; Knowles, T. P. J.; Vendruscolo, M.; Christodoulou, J.; Dobson, C. M.;

- Schenk, D.; McConlogue, L. *PLoS One* **2014**, *9*, e87133.
- (26) Allison, J. R.; Varnai, P.; Dobson, C. M.; Vendruscolo, M. *J. Am. Chem. Soc.* **2009**, *131*, 18314–18326.
- (27) Schwalbe, M.; Ozenne, V.; Bibow, S.; Jaremko, M.; Jaremko, L.; Gajda, M.; Jensen, M. R.; Biernat, J.; Becker, S.; Mandelkow, E.; Zweckstetter, M.; Blackledge, M. *Structure* **2014**, *22*, 238–249.
- (28) McColl, I. H.; Blanch, E. W.; Gill, A. C.; Rhie, A. G. O.; Ritchie, M. A.; Hecht, L.; Nielsen, K.; Barron, L. D. *J. Am. Chem. Soc.* **2003**, *125*, 10019–10026.
- (29) Wilson, G.; Ford, S. J.; Cooper, A.; Hecht, L.; Wen, Z. Q.; Barron, L. D. *J. Mol. Biol.* **1995**, *254*, 747–760.
- (30) Wilson, G.; Hecht, L.; Barron, L. D. *J. Mol. Biol.* **1996**, *261*, 341–347.
- (31) Myshakina, N. S.; Ahmed, Z.; Asher, S. A. *J. Phys. Chem. B* **2008**, *112*, 11873–11877.
- (32) Lubner, S. *J. Phys. Chem. A* **2013**, *117*, 2760–2770.
- (33) Kessler, J.; Kapitán, J.; Bouř, P. *J. Phys. Chem. Lett.* **2015**, *6*, 3314–3319.
- (34) Kessler, J.; Yamamoto, S.; Bouř, P. *Phys. Chem. Chem. Phys.* **2017**, *19*, 13614–13621.